# Kirigami-inspired organic and inorganic film-based flexible thermoelectric devices with built-in heat sink

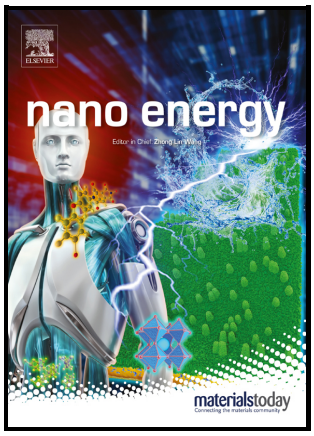


Chongyang Zeng, Kan Chen, Cevriye Koz, Eleni-Chrysanthi Stefanaki, Eugenio Sebastian Suena Galindez, Han Zhang, Oliver Fenwick, Richard Tuley, Emiliano Bilotti

PII: S2211-2855(23)01050-9

DOI: https://doi.org/10.1016/j.nanoen.2023.109213

Reference: NANOEN109213

To appear in: *Nano Energy*

Received date: 4 October 2023
Revised date: 12 November 2023
Accepted date: 16 December 2023

Please cite this article as: Chongyang Zeng, Kan Chen, Cevriye Koz, Eleni-Chrysanthi Stefanaki, Eugenio Sebastian Suena Galindez, Han Zhang, Oliver Fenwick, Richard Tuley and Emiliano Bilotti, Kirigami-inspired organic and inorganic film-based flexible thermoelectric devices with built-in heat sink, *Nano Energy,* (2023) doi:https://doi.org/10.1016/j.nanoen.2023.109213

# Kirigami-inspired organic and inorganic film-based flexible thermoelectric devices with built-in heat sink

*Chongyang Zeng [1], Kan Chen [2], Cevriye Koz [3], Eleni-Chrysanthi Stefanaki [3], Eugenio Sebastian Suena Galindez [2], Han Zhang [2], Oliver Fenwick [2], Richard Tuley [3]*, Emiliano Bilotti [1]**

[1] Department of Aeronautics, Imperial College London, Exhibition Road, London, SW7 2AZ, U.K.

[2] School of Engineering and Materials Science, Queen Mary University of London, London, E1 4NS, U.K.

[3] European Thermodynamics Ltd, 8 Priory Business Park, Wistow Road, Kibworth, Leicestershire, LE8 0RX, UK

*Corresponding authors e-mails: richard.tuley@etdyn.com; e.bilotti@imperial.ac.uk.

Abstract

Thermoelectric (TE) devices can convert heat to electricity directly, which offers a unique opportunity to realize waste heat recovery. However, conventional TE devices inevitably use heat sinks, which are bulky, rigid and heavy, limiting practical applications. Herein, we propose a fully integrated film-based TE device with intrinsically built-in fins as heat sink in a hexagonal honeycomb device structure, that simultaneously achieves high TE performance and conformability, as confirmed by experiments and modelling. A flexible Kapton substrate with copper electrodes, integrating either carbon nanotube (CNT) veils or bismuth telluride ($Bi_2Te_3$) TE 'legs', both of n- and p-type, achieved a remarkable specific power of 185.4 nW $K^{-2}$ for a $Bi_2Te_3$-based device and 53.1 nW $K^{-2}$ for a CNT-based device, thanks to the heat dissipation

effect granted by the built-in fins. Besides, the addition of oriented polymer films interconnects, contracting when above their glass transition temperature, allowed a single substrate two-dimensional (2D) TE device to self-fold into a three-dimensional (3D) hexagonal honeycomb structure, with built-in fins, contactlessly and autonomously. The demonstrated shape-programmed kirigami-inspired scalable TE device paves the way for realising self-powered applications comprising hundreds of TE legs with both inorganic (e.g., $Bi_2Te_3$) and organic (e.g. CNT veils) TE materials and integrated heat sinks.

Graphical abstract

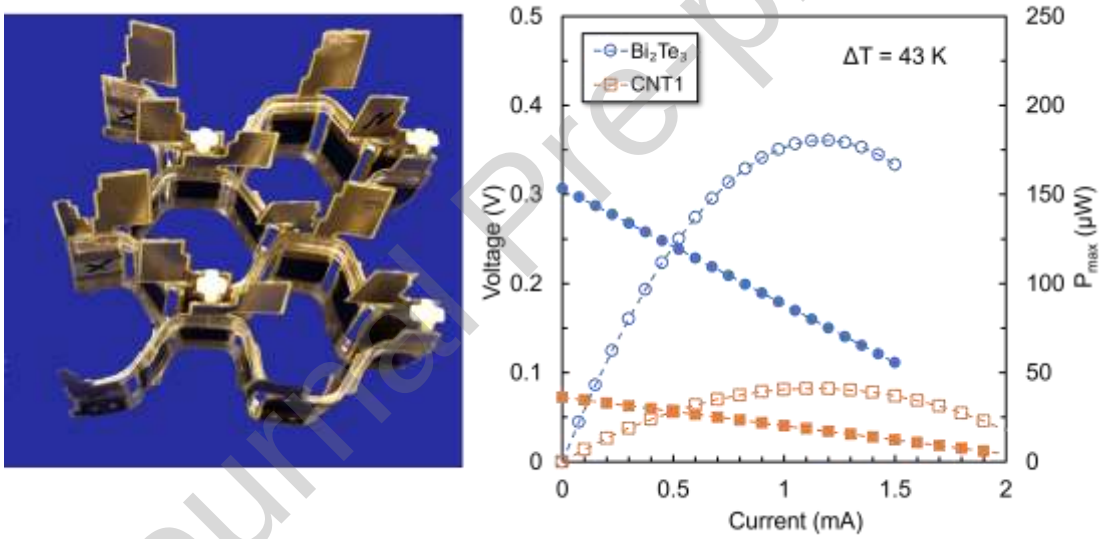


An efficient self-folded thermoelectric device, inspired by Kirigami, with built-in heat sinks and generally applicable to organic (CNTs veils) and inorganic (BiTe) thin-film materials.

Keywords: Thermoelectric device, Bismuth telluride, Carbon nanotube veil, Karigami

# 1. Introduction

Thermoelectric (TE) technology presents a unique opportunity to convert waste heat directly into electricity, offering a promising solution to address waste heat recovery and

sustainability challenges. Intense effort has been dedicated to designing and fabricating high-performance TE devices over the past few decades [1-7]. Traditional thermoelectric generators (TEGs) are fabricated by assembling individual p- and n-type TE materials into a module, which are then sandwiched between a hot source and a heat sink [8-10]. However, these conventional TEGs have several drawbacks, such as the large mass and volume, mechanical rigidity, high cost, and limited scalability. Therefore, film-based TEGs have been proposed as an alternative, which offers the advantages of flexibility, ease of manufacturing, and potential for integration with other devices [11-15].For high-performance TE materials [16], the most promising inorganic candidate is still (doped) bismuth telluride ($Bi_2Te_3$), despite significant efforts to find commercially viable alternatives [11, 17-21]. The *ZT* value (defined as $ZT = TS^2\sigma/\kappa$, which scales with the electrical conductivity ($\sigma$), the square of the Seebeck coefficient (*S*), the inverse of thermal conductivity ($\kappa$) and the material temperature (*T*)) of $Bi_2Te_3$-based material can reach about 1.8 at 320 K [22]. $Bi_2Te_3$ films and devices can be fabricated, for instance, via magnetic sputtering [11], in-situ synthesis [23] and screen-printing [24].

Organic TE materials have recently attracted significant attention owing to potentially easy and scalable processability, flexibility, mechanical robustness and use of abundant and non-toxic elements, among which carbon nanotube (CNT) and their polymer composites have seen the best TE performances [25-27]. Cho et al. fabricated polyelectrolyte carbon nanocomposites via layer-by-layer (LBL) assembling method. The LBL multilayer film consisted of polyaniline, graphene and double-walled carbon nanotubes and exhibited a remarkable power factor of 1825 $\mu W\ m^{-1}\ K^{-2}$ [28]. Choi et al. prepared a wearable and flexible TEG with all highly-aligned CNT veils, reporting a power output of 8 μW in correspondence of a temperature difference ($\Delta T$) of 50 K [8]. Very recently, Wan et al. utilised a temperature-induced self-folding process to harvest out-of-plane energy and achieved a high TE output performance of 21 mV and 812 nW at a $\Delta T$ of only 17 K based on continuous CNT veils in structural composites [29].

Regardless of the selection of TE materials, one of the biggest limitations of TEGs lies in the need of heat sinks, to thermally link the device to air during operation. Moreover, the use of radiative coolers (thermal emitters) is another way to maintain the cold side, by transferring heat to cold space [30, 31]. This requirement leads to increased mass, volume, costs and limits efficiency, which is an obstacle to their practical applications. Therefore, design and fabrication solution for high-performance TEGs, that do not rely on a rigid and external heat sink, and that can perfectly utilise the heat sources in real scenarios, is highly desirable.

Herein, we report a new configuration of an efficient TE device with a built-in heat sink. In particular, our device design is based on a hexagonal honeycomb structure, inspired by an ancient art of origami and kirigami [13], which is formed by folding up a two-dimensional (2D) flat structure, and has built-in fins, eliminating the need for external heat sinks. The same 2D flat structure, when modified with an oriented polymeric film, which contracts when exposed to a temperature above its glass transition, can contactlessly self-actuate into the 3D hexagonal honeycomb device. The thin and large fin-like structures will increase the contact area and thus heat conduction between the cold side of the thermoelectric and the external air or other media. Therefore, fins in a TE device are beneficial to promote heat transfer and help maintain a temperature gradient in the TE device. In this experiment, the fins are designed to replace the traditional rigid and external heat sinks in thermoelectric applications. Such a 3D device is robust [32] and presents better thermal coupling to air, and hence better TE performance, as demonstrated through experimental characterization and modelling. The maximum power output of a device with 76 pairs of p-n legs connected in series is 406 μW (at $\Delta T$ = 47 K), when using $Bi_2Te_3$ as the active TE material, and 119 μW (at $\Delta T$ = 52 K), when using CNTs. The output performance of the $Bi_2Te_3$-based device (185.4 nW $K^{-2}$) and the CNT-based device (53.1 nW $K^{-2}$), in particular, is superior to previously reported lateral printed $Bi_2Te_3$ and organic TEGs, directly coupled with air.

This work provides a path to optimise the thermoelectric performance of TE devices by designing rational 3D structures without the need for a bulky heat sink. The proposed approach has the potential to reduce the cost, mass, and volume of TE devices while allowing easier manufacturability and installation, making them more attractive in the chemical and petroleum industries, metal or glass manufacturing sites, for a wide range of potential applications like waste heat recovery, energy harvesting [33], cooling and thermal management.

## 2. Experimental section

### *2.1. Materials*

Carbon nanotube (CNT) veils, fabricated by the floating catalyst chemical vapor deposition method, were purchased from Suzhou Creative Nano Carbon Co., Ltd. The veils are composed of multi-walled carbon nanotubes (MWCNT) of a diameter of ~5-20 nm and an apparent density of about 0.5 g $cm^{-3}$. Iron (III) chloride ($FeCl_3$, anhydrous, 98%) was purchased from Alfa Aesar. Polyethylenimine (PEI, branched, Mw ~ 600, >99%) was purchased from Sigma-Aldrich. Ethyl cellulose (EC, ethoxyl content 48%, 10 cps) was purchased from Acros Organics. The doped bismuth telluride ($Bi_2Te_3$) ink (suspensions of $Bi_{0.4}Sb_{1.6}Te_3$ and $Bi_2Te_{2.7}Se_{0.3}$ polycrystalline powders in a proprietary blend of polymers and alcohols) and the device substrate were provided by European Thermodynamic Ltd (ETL). Grafix shrink films (polystyrene) with a thickness of 250 µm were bought from Amazon. Tesa 51408 premium grade polyimide tape (Kapton tape) and Loctite super glue (ethyl 2-cyanoacrylate) were purchased from RS components. The chemical reagents, used without further purifications, are acetone (99.5%) and ethanol (96%, v/v) purchased, respectively, from Thermo Scientific and Honeywell.

### *2.2. Fabrication of doped CNT veils*

CNT veils were cut into 1.5 cm × 1.5 cm. Then 50 μL, 10 mM $FeCl_3$ or 10 mM PEI ethanol solution were dropped onto the CNT veils for p-type or n-type doping, respectively. $FeCl_3$-doped CNT veils (p-CNT) were dried at room temperature for 4 h. PEI-doped CNT veils (n-CNT) were dried at 80 °C for 4 h. A modified preparation entailed the addition of 0.2 wt% ethyl cellulose (EC) onto the pristine (EC+CNT) and $FeCl_3$-doped CNT veils (EC+p-CNT), to improve adhesion of CNT to the electroded substrate.

### *2.3. Fabrication of TE devices*

#### *2.3.1. CNT-based TE devices*

Doped CNT veils were cut into 5 mm × 5 mm pieces, which were positioned on the electroded Kapton substrate, after which a drop of ethanol was applied and dried in ambient conditions. The electrical resistance of each CNT piece was checked by using a multimeter (Keithley 2000 multimeter), before encapsulating it with 5 mm × 10 mm Kapton tapes. After encapsulation, a TE device was formed by manual folding. For self-folded CNT device, shrinkable films of dimensions 3 mm × 20 mm and 4 mm × 16 mm, were bonded to the substrate by superglue. When the two-dimensional (2D) multilayer structure, containing encapsulated CNT veils and shrinkable films, was put into an oven, pre-heated to 135 °C, a three-dimensional (3D) TE device was formed within 30 s.

#### *2.3.2. $Bi_2Te_3$-based TE devices*

p- and n-type $Bi_2Te_3$ inks were deposited on the substrate by screen printing. First, one side of the substrate was printed with either p- or n-type ink, using a 4 × 5mm aperture screen. The printed substrate was then dried at 125 °C for 1 h and subsequently sintered at 400 °C for 1.5 h under argon atmosphere. The other type of ink was then deposited on the opposite side the substrate. Finally, double-side printed substrate was dried and sintered at 125 °C and 400

°C for 4h under argon atmosphere, respectively. The sintered inks on both sides of the substrate were encapsulated with Kapton tape before manual folding to form a TE device.

*2.4. Characterisation*

Microstructures of CNT veils and sintered $Bi_2Te_3$ were tested by a FEI Inspect F scanning electron microscope (SEM). The thickness of CNT veils was obtained by a profilometer (Bruker Dektak Vision 64). A four-probe method was used to measure the electrical resistance by using a setup which consists of a Keithley 2000 multimeter, an Agilent 6614 System DC power supply and a Keithley 6485. The Seebeck coefficient was measured at 300 K under nitrogen atmosphere by using a MMR system with a K20 digital temperature controller and a SB100 digital Seebeck controller. The thickness of the sintered $Bi_2Te_3$ films were measured by Alpha-Step D-500 stylus profiler (KLA Tencor). Room temperature electrical resistance of sintered $Bi_2Te_3$ films were measured with Jandel 4-point probe and Keithley 2400 Source Meter. A home-made Seebeck coefficent rig with DC power supply (Aim-TTi CPX Series) were utilized to measure Seebeck coefficient of $Bi_2Te_3$ films.

*2.5. Performance measurements*

*2.5.1. Output performance of TE devices*

The TE performance of both $Bi_2Te_3$-based and CNT-based TE devices was tested by a homemade test system (Fig. S1). TE devices were mounted on an aluminium metal plate (hot side) with a 2 parts thermal gap filler. The hot side temperature was measured with a PT100 sensor in the metal plate, read by a National Instruments cDAQ 9138 with 9216 module, while the cold side temperature was assumed as the air temperature, measured with a second PT100. Cartridge heaters linked to an Omega CS 8iD were used to control the hot side temperature while air flow was controlled by a variable fan and measured by a Omega FMA900A air velocity sensor connected to a NI 9205 module. The TE device under test was measured using

a Keithley 2400 Source measurement unit. The various systems and logging were coupled together using an in-house developed Labview programme.

*2.5.2. Stability of TE devices*

Thermal cycle tests were carried out by an independent test house, according to JESD22-A104-B Profile J, with 1000 temperature cycles from 0 to 100 °C, and a 5 min hold time, for both $Bi_2Te_3$-based and CNT-based TE devices.

*2.6 Simulation of the design and architecture of TE devices*

The TE device was simulated as a coupled thermal and electrical system in COMSOL Multiphysics 6.1 with AC/DC, Heat Transfer, and Optimization Modules. An approximate symmetry element consisting of 2 half couples was simulated to reduce computation time. The COMSOL optimisation study (using the BOBYQA mathematical method) was used to find the optimum load resistance for maximum power. The measured effective specific electrical contact resistances of 35 $\mu\Omega$ $cm^2$ and 17 $\mu\Omega$ $cm^2$, for $Bi_2Te_3$ and CNT materials respectively, were added as input. Fixed temperature boundary conditions of the metal base plate and air were assumed. A 2.2 W $m^{-1}$ $K^{-1}$ thermal interface material was included to aid heat transfer between the metal baseplate and the device. Thermal coupling to air was simplified by a constant heat transfer coefficient of 5 W $m^{-2}$ $K^{-1}$ for fin areas and 3 W $m^{-2}$ $K^{-1}$ for enclosed hexagonal areas, rising to 25 W $m^{-2}$ $K^{-1}$ and 15 W $m^{-2}$ $K^{-1}$, respectively, under 1.5 m $s^{-1}$ airflow.

# 3. Results and discussion

*3.1. Design of TE devices with built-in fins as heat sinks*

Natural convection conditions commonly occur for one of the temperature sources or sinks in an energy harvesting application. However, natural convection imposes a significant challenge to thermally couple the TE materials to the air. This limit is typically reduced by

using a heat sink larger than the thermoelectric device, alongside a significant increase in solid-air interface area, using heat sink fins. However, due to the low driving pressure for natural convection, the optimum fin spacing is typically large, about 5 mm [34]. Therefore, from an effective application perspective, for a device with integrated heat sink to couple to air, a tightly packed device is not a necessary requirement, and a more dispersed device puts less stringent requirements on the fin sizes and heat spreading. Therefore, the device architecture is based around a dispersed hexagonal design as illustrated in Fig. 1a. Such a design can be formed in a scalable way as it can be constructed by folding up a single flat substrate.

The whole device consists of a Kapton substrate (in blue) with copper interconnects (in purple) forming the fins and connecting the p and n TE materials (in red). Plated through holes on the interconnects allow electrical connection between both sides of substrates to maximize substrate usage. The base of the device is embedded in a thermal interface material (Kapton) to provide good thermal coupling to the metal base plate. Temperature gradients are then created parallel to the fin length direction of the substrate to enable sufficient temperature gradients to develop across the TE material (Fig. 1b).

The dependence of power output on fin length and TE length are shown in Fig. 1c and Fig. 1d for $Bi_2Te_3$ and CNT veil, respectively. It can be seen that the thermal link to air remains a challenge, with longer fin lengths improving performance. Unfortunately, there are limits on practically achievable fin lengths both to allow it to be self-supporting and to avoid the use of excessively large substrate areas, which would detrimentally increase cost. Two designs are experimentally produced in this paper, one with an effective average fin length of 4.2 mm (which corresponds to a maximum single fin height of 13.5 mm when folding restrictions on fin areas have been taken into account) and a wider fin design which acts equivalently to an average fin length of 9.1 mm. Optimum TE length (Fig. S2 and Note 1) is more material

dependent, but a common 3 mm design can be used for both materials with only modest compromise from optimum performance.

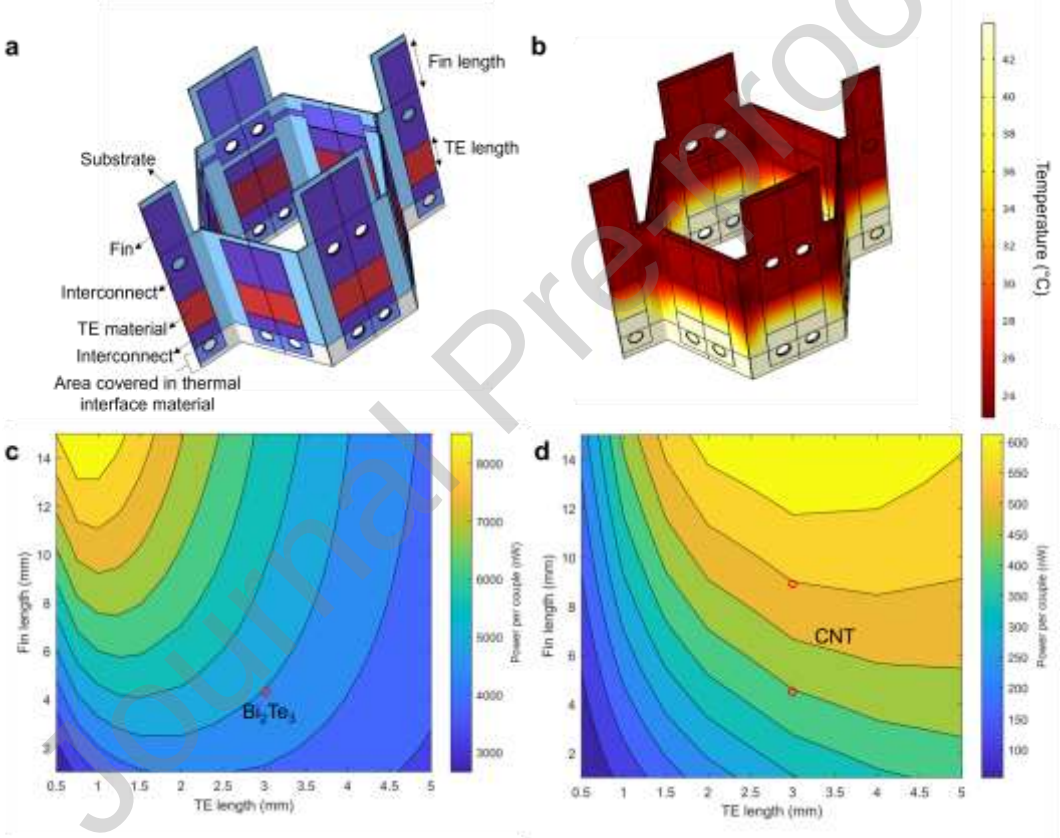


**Fig.1 Design of thermoelectric (TE) device. a** The structure of TE device. **b** Thermal distribution of designed TE device by COMSOL modelling, with 317 K base plate and 292 K air temperature. Dependence of power (per couple) on fin length and TE length under natural convection, for (**c)** for $Bi_2Te_3$, and (**d**) CNT veil.

*3.2. TE performance of CNT veils and $Bi_2Te_3$*

The p and n-type CNT veils were obtained by mild non-covalent doping. The microstructures of CNT veils did not change significantly after doping with 0.2 wt% ethyl cellulose (EC), iron (III) chloride solution ($FeCl_3$) with 0.2 wt% EC, and polyethyleneimine (PEI), except for a slight increase in apparent density (Fig. 2a-c), compared to the pristine CNT veil (Fig. S3). Here, EC was added into p-type CNT veils (EC+p-CNT) to improve the adhesion between p-type CNT veils and copper substrate (Fig. S4). For what concerns the microstructures of n-type (Fig. 2d) and p-type $Bi_2Te_3$ (Fig. 2e), all samples showed a dense surface structure after sintering at 400 °C in an argon atmosphere.

The pristine CNT veil had a thickness of about 3.5 µm and anisotropic electrical conductivity (σ), between 1159 S $cm^{-1}$ (perpendicular to the CNT alignment) and 1290 S $cm^{-1}$ (parallel to the CNT alignment, Fig. S5). CNT veil pieces were positioned with their pre-aligned direction (higher electrical conductivity) along the electrodes. Due to the screen printing method for the $Bi_2Te_3$, the thickness of n and p-type $Bi_2Te_3$ films was higher than the CNT veils, at 42 ± 10 µm and 30 ± 7 µm, respectively. Electrical conductivities of EC+p-CNT and n-CNT veils were 1752 S $cm^{-1}$ and 1231 S $cm^{-1}$, higher than the value for pristine CNT veil (1290 S $cm^{-1}$). The conductivity of EC+CNT (1102 S $cm^{-1}$) is lower that pristine CNT veils due to the addition of electrically insulating EC. The electrical conductivity values of n-$Bi_2Te_3$ and p-$Bi_2Te_3$ were 56 S $cm^{-1}$ and 510 S $cm^{-1}$, respectively. The Seebeck coefficient (*S*) of EC+CNT, EC+p-CNT and n-CNT veils were 73 µV $K^{-1}$, 54 µV $K^{-1}$ and -64 µV $K^{-1}$. While n-$Bi_2Te_3$ and p-$Bi_2Te_3$ presented a Seebeck coefficient of -206 µV $K^{-1}$ and 276 µV $K^{-1}$, about 4 times higher than that of CNT veils. Overall, the power factor of doped and undoped CNT materials ranged between 517 and 585 µW $m^{-1}$ $K^{-2}$, while it was 3895 µW $m^{-1}$ $K^{-2}$ and 230 µW $m^{-1}$ $K^{-2}$, for p- and n-type $Bi_2Te_3$, respectively. Overall, p-type $Bi_2Te_3$ possessed superior TE properties.

To investigate the effect of thermal treatment on TE performance of CNT veils, microstructures, $\sigma$ and $S$ of doped and undoped CNT veils were tested after a heat treatment at 150 °C in an oven for 1 h. The microstructures showed no obvious change with heat treatment (Fig. S6). The n-CNT veils showed stable TE properties, with a negative Seebeck coefficient maintained and unchanged electrical conductivity (Fig. S7). However, the electrical conductivity of p-CNT decreased from 2620 S $cm^{-1}$ to 1368 S $cm^{-1}$, close to the value of 1221 S $cm^{-1}$ for pristine CNT. The Seebeck coefficient of the original CNT veil was 66 µV $K^{-1}$ and then decreased to 54 µV $K^{-1}$ after p-type doping with $FeCl_3$ and returned to 66 µV $K^{-1}$ after heat treatment, suggesting that the p-doping is less stable under heat treatment. This is attributed to the decomposition of $FeCl_3$ at 150 °C [35]. Therefore, undoped CNT veils with ethyl cellulose (EC+CNT) (Fig 2a) were selected as p-legs in self-folded TE devices.

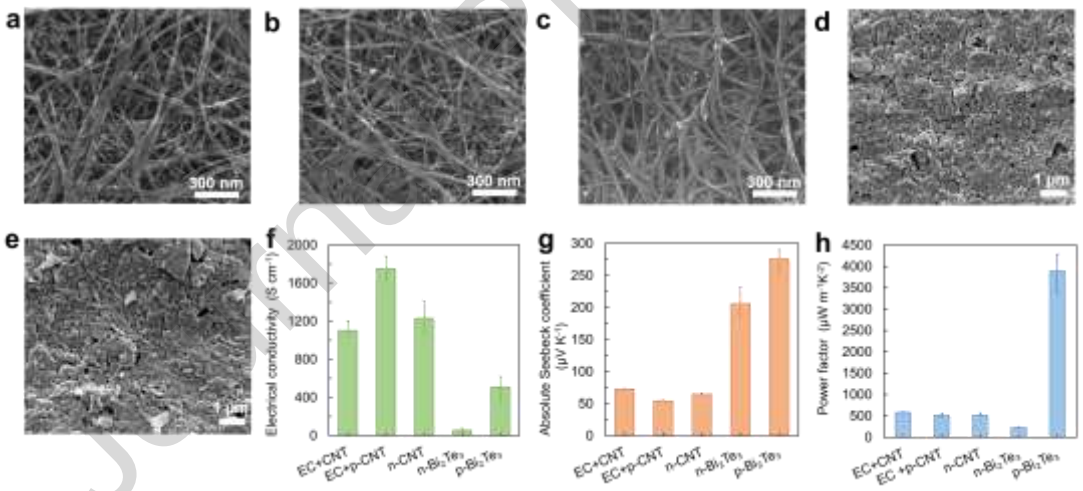


**Fig. 2 Microstructures and TE properties of doped CNT veils and $Bi_2Te_3$. a-e** SEM images of the surface of CNT veils and $Bi_2Te_3$: **a** CNT veils with 0.2 wt% ethyl cellulose (EC+CNT), **b** Iron (III) chloride ($FeCl_3$) doped CNT veils with 0.2 wt% ethyl cellulose (EC+p-CNT), **c** polyethyleneimine (PEI) doped CNT veils (n-CNT), **d** n-type $Bi_2Te_3$ (n-$Bi_2Te_3$), **e** p-type $Bi_2Te_3$ (p-$Bi_2Te_3$). Scale bars, 300 nm and 1 µm, respectively. **f-h** Electrical conductivity, Seebeck coefficient and power factor of CNT veils and $Bi_2Te_3$.

*3.3 TE performance of CNT-based and $Bi_2Te_3$-based devices*

Two kinds of TE devices were fabricated with bismuth telluride ($Bi_2Te_3$) ink and CNT veils, respectively. $Bi_2Te_3$-based devices were prepared by screen printing followed by drying and sintering, before encapsulation with Kapton tape (section 2.3). CNT-based devices were fabricated by directly positioning pieces of CNT veils on the electroded substrate, followed by encapsulation with Kapton tape. Both flat devices were then manually folded, along 60° and 180° bend lines, to form the 3D honeycomb structure (Fig. 3a). The total electrical resistance of CNT-based devices only slightly increased from 32.8 Ω to 33.3 Ω with manual folding, a negligible 1.5% variation (Fig. S8). However, the $Bi_2Te_3$-based device suffered a more significant degradation of electrical properties, with an average increase in resistance of 101% upon folding. The maximum power output of the device was measured by a homemade testing system (Fig. S1), with the ΔT measured between the metal base plate and air. With a ΔT of 43 K, the open circuit voltage and the maximum output power of the $Bi_2Te_3$-based device were 0.31 V and 180 μW, 4.4 times higher than the CNT-based device (CNT1), which was 0.07 V and 41 μW, respectively (Fig. 3b). Overall, the $Bi_2Te_3$ device demonstrated superior power and voltage due to its higher thermoelectric properties, but with the use of around 8 times more TE materials than CNT veils. Fig 3c-d demonstrate the typical parabolic dependence of power with temperature difference and linear dependence of voltage, in moderate agreement with the initial model, once folding losses in resistance are taken into account. Note that the results shown here are for reduced forced air flow of 1.5 m $s^{-1}$, due to better defined test conditions, such as air temperature, and reduced influence from the environment. In true natural convection conditions, under this enclosed configuration, power dropped on average 68% and 76%, respectively, for $Bi_2Te_3$ and CNT devices, indicating the sensitivity to the air interface (Fig. S9 and Table S1),

with a smaller proportion of the temperature difference across the thermoelectric material in this case.

After we tested the single TE device, four devices with a total of 76 p-n pair legs connected in series were measured in a similar way to test the device scalability but with a larger base-plate (Fig. S10). Both $Bi_2Te_3$ and CNT devices show significantly higher maximum power output than single devices under 2.5 m $s^{-1}$ air flow (Fig. 3e-f and Table S2): 406 μW (ΔT =47 K) and 143.5 μW (ΔT =52 K), respectively, with the load resistance of 685 Ω and 130 Ω. Although the airflow for the larger demonstrator (2.5 m $s^{-1}$) is slightly higher than in the case of airflow tests (1.5 m $s^{-1}$), results on the smaller devices suggest that airflows higher than 1.5 m $s^{-1}$ may only give 1-2% improvement in performance (Fig. S11). These results show the resistance scaling by nearly 4.4 and 5 times for the CNT and $Bi_2Te_3$, respectively, demonstrating the potential for device scalability.

Device robustness is also crucial for real-world application. Initial lifetime data was collected by performing one of the harshest lifetime tests of thermal cycling. Although the $Bi_2Te_3$-based device had better TE performance, thermal cycling tests results indicated a larger variation of the normalized resistance of $Bi_2Te_3$-based device during 1000 cycles (106% change), while the CNT-based device (CNT1) was more stable, with only 20% variation after 1000 cycles (Fig. 3g). Therefore, CNT-based devices will be more suitable for long term use in real scenarios.

While power per unit cost is likely one of the most crucial metrics, its accurate estimation is difficult. Therefore, we considered two of the more commonly reported metrics, output power and power density, as important criteria to evaluate the performance of TEGs, by respectively providing information on the scalability and the efficient use of the thermoelectric material, one of the likely more expensive components. Here, the power density is described

as the output power per TE material area. To eliminate the effect of different reported temperature differences, all output powers and power densities are normalized by the square of the temperature difference ($\Delta T^2$) [13], as only a weak temperature dependence of the material parameters is expected over these small temperature ranges. The output performance of our $Bi_2Te_3$ (185 nW $K^{-2}$) was superior to previously reported lateral printed $Bi_2Te_3$ devices. Also, our CNT 76 p-n pairs devices (53 nW $K^{-2}$) are competitive with previously reported CNT TEGs [18, 21, 32, 36-42] (Fig. 3h). The power density/$\Delta T^2$ of the $Bi_2Te_3$ with 76 p-n pairs device was 6.8 nW $mm^{-2}$ $K^{-2}$, which is close to the state of the art values of lateral devices reported in literature. The CNT 76 p-n pairs device showed a superior output performance, with the power density/$\Delta T^2$ of 20 nW $mm^{-2}$ $K^{-2}$, which is the best among the CNT literature [3, 5, 25, 27, 43-50] (Fig. 3i) and competitive even with previously reported inorganic TE devices. Therefore, this architecture allows simultaneous state of the art total power output as well as power density while being applicable to two very different materials. In addition, this has been achieved in an application orientated manner with one of the temperatures measured in air rather than on the device/metal plate, which is much more common but less meaningful in practical use. The most competitive literature reported results test the temperature difference across the device alone without this heat sink loss, typically giving an additional ~4 fold power increase from a well optimised system.

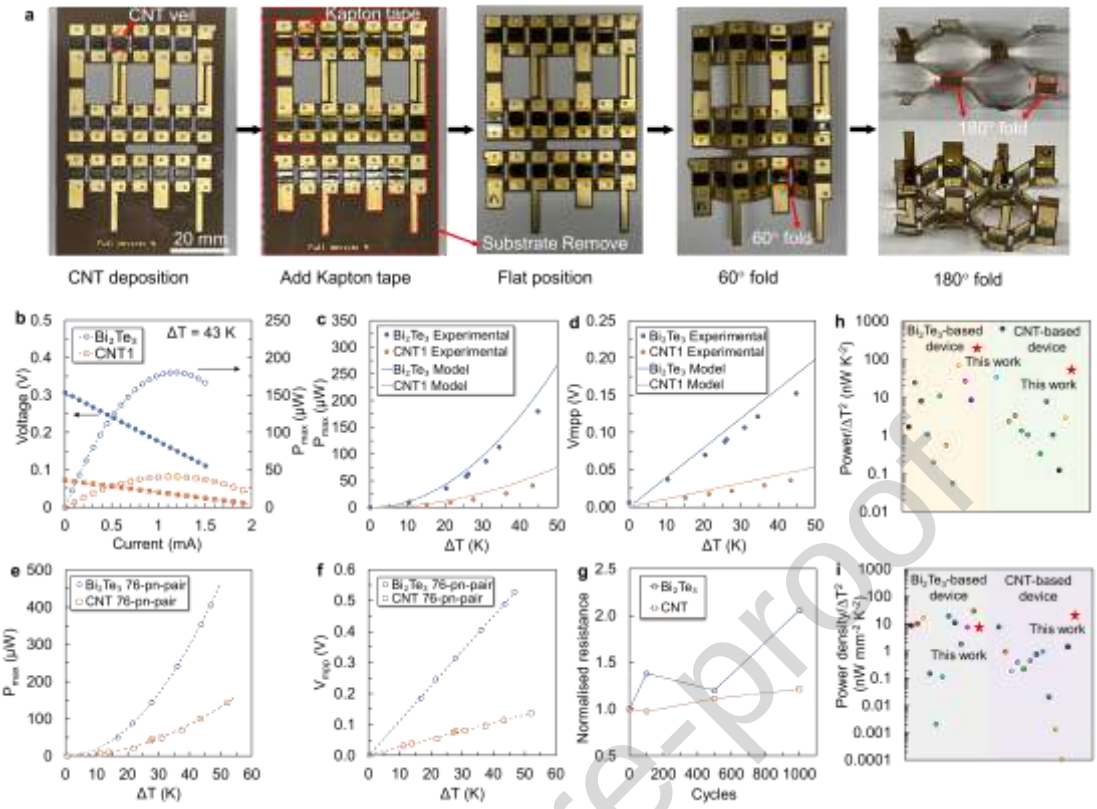


**Fig. 3 TE performance of manually folded TE devices. a** Fabrication process of a folded TE device with CNT veils. **b** TE performance comparison of $Bi_2Te_3$-based device and CNT-based device at $\Delta T = 43$ K. **c-d** Maximum power output and voltage at maximum power point of 19 p-n pairs CNT-based and $Bi_2Te_3$-based devices under different temperature gradients, setting with airflow cooling with air speed of 1.5 m $s^{-1}$ when testing. **e-f** Maximum power output and voltage at maximum power point of four CNT-based devices which are connected in series. **g** Stability of CNT-based and $Bi_2Te_3$-based devices within 1000 thermal cycle tests. **h-i** Output power and maximum power density normalized to temperature difference squared $\Delta T^2$ of our device compared with most representative literature data. The power density shown here is expressed as the power output per unit cross-sectional area. Details of calculation are reported in Supplementary Table S3 and Table S4.

*3.4. Enhanced TE performance via changing fin structures*

The modelling results (Section 3.1) suggest that the length of fins will have a significant effect on power output for one pair of p-n legs. Here, the layout of the fins is optimised to enhance the whole device's TE performance by widening the fins without utilising more total substrate area, as shown in Fig 4. When the ΔT is 50 K, the maximum power output of three CNT-based TE devices (CNT_no fins, CNT_small fins and CNT_large fins) was 21 μW, 25 μW and 40 μW, respectively, under the airflow speed of 1.5 m $s^{-1}$, 2.6 to 3.3 times higher than the same devices are under natural convection (8 μW, 12 μW and 13 μW, Fig. S12). This proves that the maximum power output increased by 90% and 50%, under two test conditions, after optimising the fin structures. Wide fins improve the contact area to air, so decreasing the temperature difference lost across this interface, keeping higher temperature difference across the thermoelectric material, and hence improving power output compared to the small fin structure.

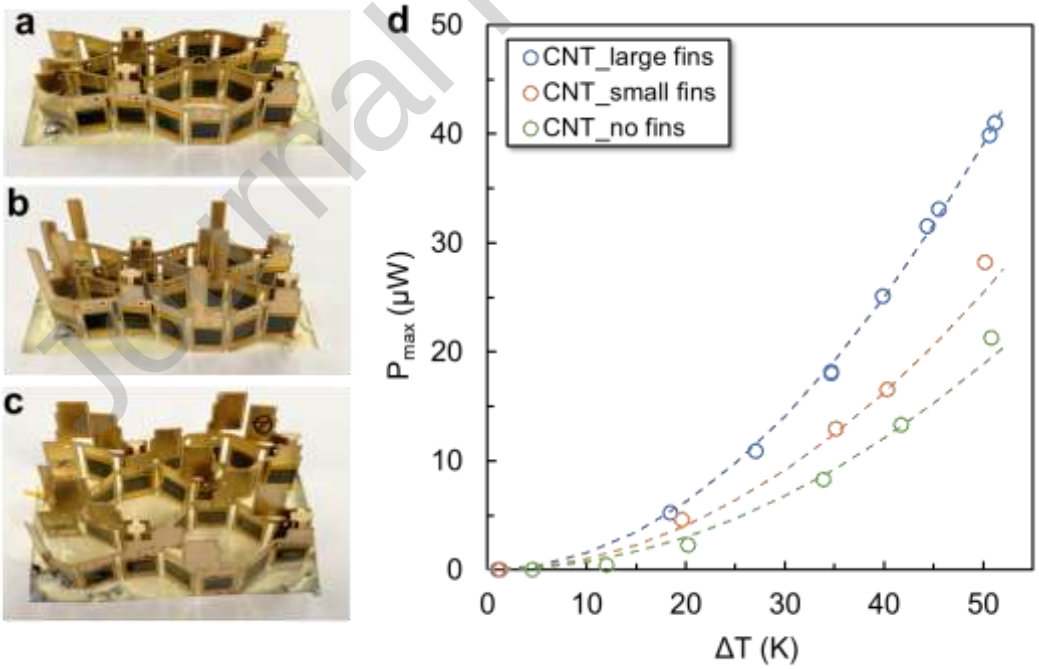

**Fig. 4 TE performance of CNT-based device with different fin design. a-c** Picture of CNT-based TE devices with no fins (**a**), small fins (**b**) and wide fins (**c**). **d** TE performance comparison.

*3.5. Self-folded TE device via kirigami*

As mentioned before, oriented polymeric films attached to the substrate can contract when heated above their glass transition temperature, which can be used as an actuation mechanism [51]. A self-folded device with optimised fins was obtained by adding shrinkable films (Fig. 5a and Video S1). When the flat substrate contacts a hot surface (>135 °C), it can self-fold to form a three-dimensional (3D) structure autonomously, which can better make use of orthogonal temperature gradients. This kind of contactless shape programming could be beneficial in some application like packaging, when deployable devices and structures are particularly desirable. The self-folded CNT-based TE device at ΔT of 50 K under the airflow and NC condition exhibited a maximum power output of 25 μW and 14 μW, respectively, and a $V_{mpp}$ of 53 mV and 42 mV (Fig. S13b-c). The maximum output power trend of the manual-folded and self-folded device, under natural convection conditions, show good agreement, indicating that the self-folded process does not alter the device TE performance (Fig. 5b), and it is stable (Fig. S14).

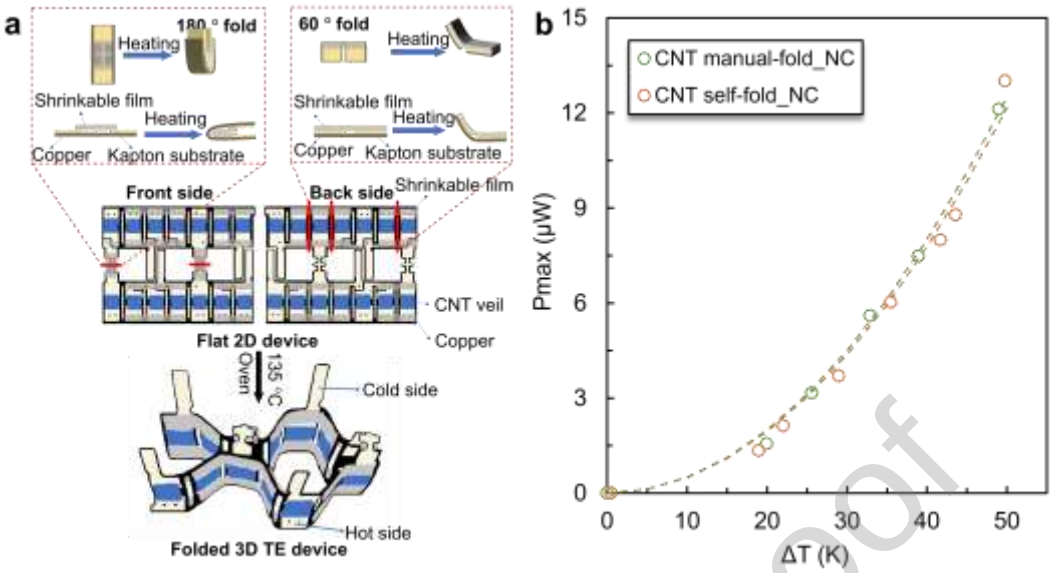


**Fig. 5 Self-folded CNT-based device and its TE performance. a** Fabrication process of a self-folded thermoelectric TE device. **b** TE performance comparison of manual-folded device and self-folded device, respectively.

## 4. Conclusion

A new film-based TEGs architecture has been developed, showing competitive power and power density performance for both inorganic and organic TE materials. This has been demonstrated in an application orientated manner utilising a built-in heat sink to efficiently couple the device to air as one of the temperature sources or sinks. The distributed honeycomb structure can be scalably folded from a single substrate, either manually or self-folded via a kirigami-inspired folding actuation without loss of performance. Such self-folding can aid contactless manufacturing, miniaturisation, and device deployment. COMSOL modelling has guided the optimisation of the device architecture with a suitable leg length and fin length, with a demonstrated 50-90% power gains. The $Bi_2Te_3$ device can generate a voltage of 0.53 V and a power output of at 406 μW at $\Delta T = 47$ K. The CNT device can generate a voltage of 0.14 V

and a power output of at 144 μW at $\Delta T$ = 52 K. While the $Bi_2Te_3$ device produces a higher output power, the CNT device produces a superior power density/$\Delta T^2$ of 20 nW $mm^{-2}$ $K^{-2}$ which is superior to previously reported CNT-based TEGs and even competitive with inorganic TEGs. In addition, the CNT device demonstrates improved robustness under thermal cycling than the $Bi_2Te_3$ device. It is believed that this work could promote the rational design of TEGs, which will significantly benefit future research and broaden the range of applications.

CRediT authorship contribution statement

**Chongyang Zeng**: Methodology, Data Curation, Investigation, Formal analysis, Writing-Original Draft. **Kan Chen**: Methodology, Investigation, Data Curation, Writing-Review & Editing. **Cevriye Koz**: Investigation, Data Curation, Formal analysis, Writing-Review & Editing. **Eleni-Chrysanthi Stefanaki**: Investigation, Data Curation. **Eugenio Sebastian Suena Galindez**: Investigation. **Oliver Fenwick**: Investigation. **Han Zhang**: Writing-Review & Editing. **Richard Tuley**: Conceptualization, Funding Acquisition, Supervision, Methodology, Writing-Review & Editing. **Emiliano Bilotti**: Conceptualization, Funding Acquisition, Supervision, Methodology, Writing-review and editing.

Declaration of Competing Interest

The authors declare that they have no known competing financial interests or personal relationships that could have appeared to influence the work reported in this paper.

Acknowledge

The authors would like to thank the support from UKRI Innovate UK (KiriTEG Project, Reference: 51868). The authors would like to acknowledge Hannah Hunter for assistance with taking photos of different TE devices. C.Z. acknowledges PhD scholarship funding from the China Scholarship Council.

Appendix A. Supporting information

Supplementary data associated with this article can be found in the online version.

**References**

[1] Z.J. Chen, H.C. Lv, Q.C. Zhang, H.F. Wang, G.M. Chen, Construction of a cement-rebar nanoarchitecture for a solution-processed and flexible film of a $Bi_2Te_3$/CNT hybrid toward low thermal conductivity and high thermoelectric performance, Carbon Energy. 4 (2022) 115-128.

[2] B. Wu, Y. Guo, C.Y. Hou, Q.H. Zhang, Y.G. Li, H.Z. Wang, High-performance flexible thermoelectric devices based on all-inorganic hybrid films for harvesting low-grade heat, Adv. Funct. Mater. 29 (2019) 1900304.

[3] X. Sun, Y.Z. Wang, K.C. Li, J. Wang, X. Dai, D.T. Chong, J.J. Yan, H. Wang, Anisotropic electrical conductivity and isotropic seebeck coefficient feature induced high thermoelectric power factor > 1800 μW $m^{-1}$ $K^{-2}$ in MWCNT films, Adv. Funct. Mater. 32 (2022) 2203080.

[4] T.P. Ding, K.H. Chan, Y. Zhou, X.Q. Wang, Y. Cheng, T.T. Li, G.W. Ho, Scalable thermoelectric fibers for multifunctional textile-electronics, Nat. Commun. 11 (2020) 6006.

[5] T.T. Sun, B.Y. Zhou, Q. Zheng, L.J. Wang, W. Jiang, G.J. Snyder, Stretchable fabric generates electric power from woven thermoelectric fibers. Nat. Commun. 11 (2020) 572.

[6] L. Liu, J. Chen, L.R. Liang, L. Deng, G.M. Chen, A PEDOT:PSS thermoelectric fiber generator. Nano Energy. 102 (2022) 107678.

[7] S.J. Jung, J. Shin, S.S. Lim, B Kwon, S.H. Baek, S.K. Kim, H.H. Park, J.S. Kim, Porous organic filler for high efficiency of flexible thermoelectric generator. Nano Energy. 81 (2021) 105604.

[8] J. Choi, Y. Jung, C.C. Dun, K.T. Park, M.P. Gordon, K. Haas, P.Y. Yuan, H. Kim, C.R. Park, J.J. Urban. High-performance, wearable thermoelectric generator based on a highly aligned carbon nanotube sheet. Acs Appl. Energy Mater. 3 (2020) 1199-1206.

[9] A. Nozariasbmarz, R.A. Kishore, B. Poudel, U. Saparamadu, W.J. Li, R. Cruz, S. Priya, High power density body heat energy harvesting. Acs Appl. Mater. Interfaces. 11 (2019) 40107-40113.

[10] G. Lee, C.S. Kim, S. Kim, Y.J. Kim, H. Choi, B.J. Cho, Flexible heatsink based on a phase-change material for a wearable thermoelectric generator. Energy.179 (2019) 12-18.

[11] Q. Jin, S. Jiang, Y. Zhao, D. Wang, J.H. Qiu, D.M. Tang, J. Tan, D.M. Sun, P.X. Hou, X.Q. Chen, K.P. Tai, N. Gao, C. Liu, H.M. Cheng, X. Jiang, Flexible layer-structured $Bi_2Te_3$ thermoelectric on a carbon nanotube scaffold. Nat. Mater. 18 (2019) 62-68.

[12] H. An, M. Pusko, D. Chun, S. Park, J. Moon, In-situ synthesis of flexible hybrid composite films for improved thermoelectric performance. Chem. Eng. J. 357 (2019) 547-558.

[13] Z.P. Guo, Y.D. Yu, W. Zhu, Q.Q. Zhang, Y.T. Liu, J. Zhou, Y.L. Wang, J. Xing, Y. Deng, Kirigami-based stretchable, deformable, ultralight thin-film thermoelectric generator for bodyNET application. Adv. Energy Mater. 12 (2021) 2102993.

[14] Z.H. Zheng, X.L. Shi, D.W. Ao, W.D. Liu, M. Li, L.Z. Kou, Y.X. Chen, F. Li, M. Wei, G.X. Liang, P. Fan, G.Q. Lu, Z.G. Chen. Harvesting waste heat with flexible $Bi_2Te_3$ thermoelectric thin film. Nat. Sustain. 6 (2023) 180-191.

[15] J.G. Shi, X.L. Wu, X.J. Geng, L.P. Hu, F.S. Liu, W.Q. Ao, C.H. Zhang, Anisotropy engineering in solution-derived nanostructured $Bi_2Te_3$ thin films for high-performance flexible thermoelectric devices. Chem. Eng. J. 458 (2023) 141450.

[16] Z.H. Wu, S. Zhang, Z.K. Liu, E.Z Mu, Z.Y. Hu, Thermoelectric converter: strategies from materials to device application. Nano Energy. 91 (2022) 106692.

[17] D.L. Qin, F. Pan, J. Zhou, Z.B. Xu, Y. Deng, High ZT and performance controllable thermoelectric devices based on electrically gated bismuth telluride thin films. Nano Energy, 89 (2021) 106472.

[18] D. W. Ao, W.D. Liu, Z.H. Zheng, X.L. Shi, M. Wei, Y.M. Zhong, M. Li, G.X. Liang, P. Fan, Z.G. Chen, Assembly-free fabrication of high-performance flexible inorganic thin-film thermoelectric device prepared by a thermal diffusion. Adv. Energy Mater. 12 (2022) 2202731.

[19] J.F. Yuan, R. Zhu, A fully self-powered wearable monitoring system with systematically optimized flexible thermoelectric generator. Appl. Energy, 271 (2020) 115250.

[20] B. Lee, H. Cho, K.T. Park, J.S. Kim, M. Park, H. Kim, Y. Hong, S. Chung, High-performance compliant thermoelectric generators with magnetically self-assembled soft heat conductors for self-powered wearable electronics. Nat. Comm. 11 (2020) 5948.

[21] S.H. Park, S. Jo, B. Kwon, F. Kim, H.W. Ban, J.E. Lee, D.H. Gu, S.H. Lee, Y. Hwang, J.S. Kim, D.B. Hyun, S. Lee, K.J. Choi, W. Jo, J.S. Son, High-performance shape-engineerable thermoelectric painting. Nat. Commun.7 (2016) 13403.

[22] S.I. Kim, K.H. Lee, H.A. Mun, H.S. Kim, S.W. Hwang, J.W. Roh, D.J. Yang, W.H. Shin, X.S. Li, Y.H. Lee, G.J. Snyder, S.W. Kim, Dense dislocation arrays embedded in grain boundaries for high-performance bulk thermoelectrics. Science. 348 (2015) 109-114.

[23] X.N. Chen, L.N. Feng, P.L. Yu, C. Liu, J.L. Lan, Y.H. Lin, X.P. Yang, Flexible thermoelectric films based on $Bi_2Te_3$ nanosheets and carbon nanotube network with high n-Type performance. Acs Appl. Mater. Interfaces. 13 (2021) 5451-5459.

[24] A. Amin, R. Huang, D. Newbrook, V. Sethi, S. Yong, S. Beeby, I. Nandhakumar, Screen-printed bismuth telluride nanostructured composites for flexible thermoelectric applications. J. Phys. Energy, 4 (2022) 024003.

[25] W.B. Zhou, Q.X. Fan, Q. Zhang, L. Cai, K.W. Li, X.G. Gu, F. Yang, N. Zhang, Y.C. Wang, H.P. Liu, W.Y. Zhou, S.S. Xie, High-performance and compact-designed flexible thermoelectric modules enabled by a reticulate carbon nanotube architecture. Nat. Commun. 8 (2017) 14886.

[26] H. Zhan, Y.W. Chen, Q.Q. Shi, Y. Zhang, R.W. Mo, J.N. Wang, Highly aligned and densified carbon nanotube films with superior thermal conductivity and mechanical strength. Carbon. 186 (2022) 205-214.

[27] B. Wu, Y. Guo, C.Y. Hou, Q.H. Zhang, Y.G. Li, H.Z. Wang, From carbon nanotubes to highly adaptive and flexible high-performance thermoelectric generators. Nano Energy. 89 (2021) 106487.

[28] C. Cho, B. Stevens, J.H. Hsu, R. Bureau, D.A. Hagen, O. Regev, C. Yu, J.C. Grunlan, Completely organic multilayer thin film with thermoelectric power factor rivaling inorganic tellurides. Adv. Mater. 27 (2015) 2996-3001.

[29] K.N. Wan, A. Kernin, L. Ventura, C.Y. Zeng, Y.S. Wang, Y. Liu, J.J. Vilatela, W.B. Lu, E. Bilotti, H. Zhang. Toward self-powered sensing and thermal energy harvesting in high-performance composites via self-folded carbon nanotube honeycomb structures. Acs Appl. Mater. Interfaces. 15 (2023) 44212-44223.

[30] E.Z. Mu, Z.H. Wu, Z.M. Wu, X. Chen, Y. Liu, X.C. Fu, Z.Y. Hu, A novel self-powering ultrathin TEG device based on micro/nano emitter for radiative cooling. Nano Energy. 55(2019) 495-500.

[31] S. Zhang, Z.H. Wu, Z.K. Liu, Z.Y. Hu, An emerging energy technology: self-uninterrupted electricity power harvesting from the sun and cold space. Adv. Energy Mater. 13 (2023) 2300260.

[32] X. Zhao, W.J. Han, Y.F. Jiang, C.S. Zhao, X.X. Ji, F.G. Kong, W.Y. Xu, X. Zhang, A honeycomb-like paper-based thermoelectric generator based on a $Bi_2Te_3$/bacterial cellulose nanofiber coating. Nanoscale. 11 (2019) 17725-17735.

[33] P. Vincenzo, S. R. P. Silva, J. D. Phillips, E. Artegiani, A. Romeo, H. Shim, J. Park, J. H. Kim, J. S. Yun, G. C. Welch, et al, Roadmap on energy harvesting materials. J. Phys. Mater. 6 (2023) 042501.

[34] H. Lee, Thermal design: heat sinks, thermoelectrics, heat pipes, compact heat exchangers, and solar cells, John Wiley & Sons, 2022.

[35] S.B. Kanungo, S.K. Mishra, Thermal dehydration and decomposition of $FeCl_3 \cdot xH_2O$, J. Therm. Anal. 46 (1996) 1487-1500.

[36] T. Varghese, C. Hollar, J. Richardson, N. Kempf, C. Han, P. Gamarachchi, D. Estrada, R.J. Mehta, Y.L. Zhang, High-performance and flexible thermoelectric films by screen printing solution-processed nanoplate crystals. Sci. Rep. 6 (2016) 33135.

[37] M.M. Mallick, L. Franke, A.G. Rösch, S. Ahmad, H. Geßwein, Y.M. Eggeler, M. Rohde, U. Lemmer, Realizing high thermoelectric performance of Bi-Sb-Te-Based Printed films through grain interface modification by an in situ-grown beta-Cu(2-delta)Se Phase. ACS Appl. Mater. Interfaces. 13 (2021) 61386-61395.

[38] H.Y. Fang, B.C. Popere, E.M. Thomas, C.K. Mai, W.B. Chang, G.C. Bazan, M.L. Chabinyc, R.A. Segalman, Large-scale integration of flexible materials into rolled and corrugated thermoelectric modules. J. Appl. Polym. Sci. 134 (2017) 44208.

[39] M. Saeidi-Javash, W. Kuang, C.C. Dun, Y.L. Zhang, 3D Conformal printing and photonic sintering of high-performance flexible thermoelectric films using 2D nanoplates. Adv. Funct. Mater. 29 (2019) 1901930.

[40] D.P. Wang, S.F. Zhao, R.Y. Yin, L.L. Li, Z. Lou, G.Z. Shen, Recent advanced applications of ion-gel in ionic-gated transistor. Npj Flex. Electron. 5 (2021) 13.

[41] D. Madan, Z.Q. Wang, A. Chen, R. Winslow, P.K. Wright, J.W. Evans, Dispenser printed circular thermoelectric devices using Bi and $Bi_{0.5}Sb_{1.5}Te_3$. Appl. Phys. Lett. 104 (2014) 013902.

[42] T. Varghese, C.C. Dun, N. Kempf, M. Saeidi-Javash, C. Karthik, J. Richardson, C. Hollar, D. Estrada, Y.L. Zhang, Flexible thermoelectric devices of ultrahigh power factor by scalable printing and interface engineering. Adv. Funct. Mater. 30 (2020) 1905796.

[43] G.B. Wu, Z.G. Zhang, Y.F. Li, C.Y. Gao, X. Wang, G.M. Chen, Exploring high-performance n-Type thermoelectric composites using amino-substituted rylene dimides and carbon nanotubes. ACS Nano. 11 (2017) 5746-5752.

[44] L.M. Wang, Q. Yao, J.X. Xiao, K.Y. Zeng, S.Y. Qu, W. Shi, Q. Wang, L.D. Chen, Engineered molecular chain ordering in single-walled carbon nanotubes/polyaniline composite films for high-performance organic thermoelectric materials. Chem. Asian J. 11 (2016) 1804-1810.

[45] K.K. Jung, Y. Jung, C.J. Choi, J.M. Lee, J.S. Ko, Flexible thermoelectric generator with polydimethyl siloxane in thermoelectric material and substrate. Curr. Appl. Phys. 16 (2016) 1442-1448.

[46] Y.Z. Wang, Z.X. Lu, Q.J. Hu, X. Qi, Q. Li, Z.P. Wu, H.L. Zhang, C.H. Yu, H. Wang, Mass-produced metallic multiwalled carbon nanotube hybrids exhibiting high N-type thermoelectric performances. J. Mater. Chem. A. 9 (2021) 3341-3352.

[47] M.H. Lee, Y.H. Kang, J. Kim, Y.K. Lee, S.Y. Cho, Freely shapable and 3D porous carbon nanotube foam using rapid solvent evaporation method for flexible thermoelectric power generators. Adv. Energy Mater. 9 (2019) 1900914.

[48] Z.M. Zhang, B.R. Wang, J.J. Qiu, S.R. Wang, Roll-to-roll printing of spatial wearable thermoelectrics. Manuf. Lett. 21 (2019) 28-34.

[49] K. Suemori, S. Hoshino, T. Kamata, Flexible and lightweight thermoelectric generators composed of carbon nanotube-polystyrene composites printed on film substrate. Appl. Phys. Lett. 103(2013) 153902.

[50] S. Hata, K. Maeshiro, M. Shiraishi, S. Yasuda, Y. Shiozaki, K. Kametani, Y. Du, Y. Shiraishi, N. Toshima, Water-resistant organic thermoelectric generator with >10 μW output. Carbon Energy, 5(2022).

[51] A. Kernin, L. Ventura, A. Soul, K. Chen, K.N. Wan, W.B. Lu, P. Steiner, C. Kocabas, D. Papageorgiou, S. Goutianos, H. Zhang, E. Bilotti, Kirigami inspired shape programmable and reconfigurable multifunctional nanocomposites for 3D structures. Mater. Des. 224 (2022) 111335.

CRediT authorship contribution statement

**Chongyang Zeng**: Methodology, Data Curation, Investigation, Formal analysis, Writing-Original Draft. **Kan Chen**: Methodology, Investigation, Data Curation, Writing-Review & Editing. **Cevriye Koz**: Investigation, Data Curation, Formal analysis, Writing-Review & Editing. **Eleni-Chrysanthi Stefanaki**: Investigation, Data Curation. **Eugenio Sebastian Suena Galindez**: Investigation. **Oliver Fenwick**: Investigation. **Han Zhang**: Writing-Review & Editing. **Richard Tuley**: Conceptualization, Funding Acquisition, Supervision, Methodology, Writing-Review & Editing. **Emiliano Bilotti**: Conceptualization, Funding Acquisition, Supervision, Methodology, Writing-review and editing.

**Declaration of interests**

☒ The authors declare that they have no known competing financial interests or personal relationships that could have appeared to influence the work reported in this paper.

☐The authors declare the following financial interests/personal relationships which may be considered as potential competing interests:

Highlights

- A new efficient thermoelectric device with built-in heat sinks, inspired by Kirigami.
- General applicability to film-based organic and inorganic thermoelectric materials.
- Contactless shape programming process of creating the new device architecture.